Research Article

Optimized TrkB Agonist Ameliorates Alzheimer's Disease Pathologies and Improves Cognitive Functions via Inhibiting Delta-Secretase

Chun Chen, Eun H. Ahn, Xia Liu, Zhi-Hao Wang, Shilin Luo, Jianming Liao, and Keqiang Ye*
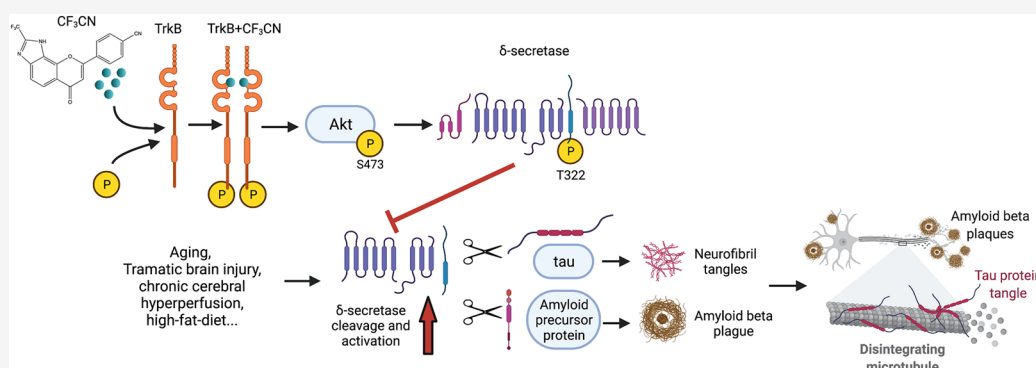
Cite This: ACS Chem. Neurosci. 2021, 12, 2448−2461

Read Online

ACCESS | Metrics & More | Article Recommendations | SI Supporting Information

ABSTRACT: BDNF/TrkB neurotropic pathway, essential for neural synaptic plasticity and survival, is deficient in neurodegenerative diseases including Alzheimer's disease (AD). Our previous works support that BDNF diminishes AD pathologies by inhibiting delta-secretase, a crucial age-dependent protease that simultaneously cleaves both APP and Tau and promotes AD pathologies, via Akt phosphorylation. Small molecular TrkB receptor agonist 7,8-dihydroxyflavone (7,8-DHF) binds and activates the receptor and its downstream signaling, exerting therapeutic efficacy toward AD. In the current study, we optimize 7,8-DHF pharmacokinetic characteristics via medicinal chemistry to obtain a synthetic derivative CF_3CN that interacts with the TrkB LRM/CC2 domain. CF_3CN possesses improved druglike features, including oral bioavailability and half-life, compared to those of the lead compound. CF_3CN activates TrkB neurotrophic signaling in primary neurons and mouse brains. Oral administration of CF_3CN blocks delta-secretase activation, attenuates AD pathologies, and alleviates cognitive dysfunctions in 5xFAD. Notably, chronic treatment of CF_3CN reveals no demonstrable toxicity. Hence, CF_3CN represents a promising preclinical candidate for treating the devastating neurodegenerative disease.

KEYWORDS: CF_3CN, BDNF, delta-secretase, Alzheimer's disease, neuroprotection

■ INTRODUCTION

Alzheimer's disease (AD) is the most common neurodegenerative disease. Its hallmark pathologic features include intraneuronal neurofibrillary tangles (NFTs), composed of hyperphosphorylated and truncated Tau, and extracellular senile plaques consisting of amyloid β (Aβ) peptides. In addition to senile plaques and NFT deposition, microglia activation associated with extensive neuroinflammation and massive neural cell death are also the prominent pathological characteristics for AD.[1] Amyloid β peptides are generated from amyloidogenic cleavage of APP (amyloid precursor protein), which is sequentially truncated by BACE1 (β-secretase 1) and γ-secretase.[2] Recently, we have reported that AEP (asparagine endopeptidase, gene name legumain: LGMN) acts as delta-secretase that simultaneously cleaves both APP and Tau and promotes amyloid deposition and NFT pathologies in AD.[3,4] Delta-secretase shreds APP at N373 and N585 sites and allows

BACE1 readily to get access to the truncated APP C-terminal fragment (amino acids (a.a.) 586−695, C110), escalating Aβ peptide production. Knockout of AEP from 5xFAD mice diminishes amyloid aggregation, attenuating cognitive disorders. APP N585 fragment is also detectable and enhanced in human AD patient brains.[4] Delta-secretase cuts Tau at N255 and N368 residues and abolishes its microtubule binding capabilities, facilitating its aggregation and neurotoxicities. Deletion of delta-secretase from Tau P301S mice substantially
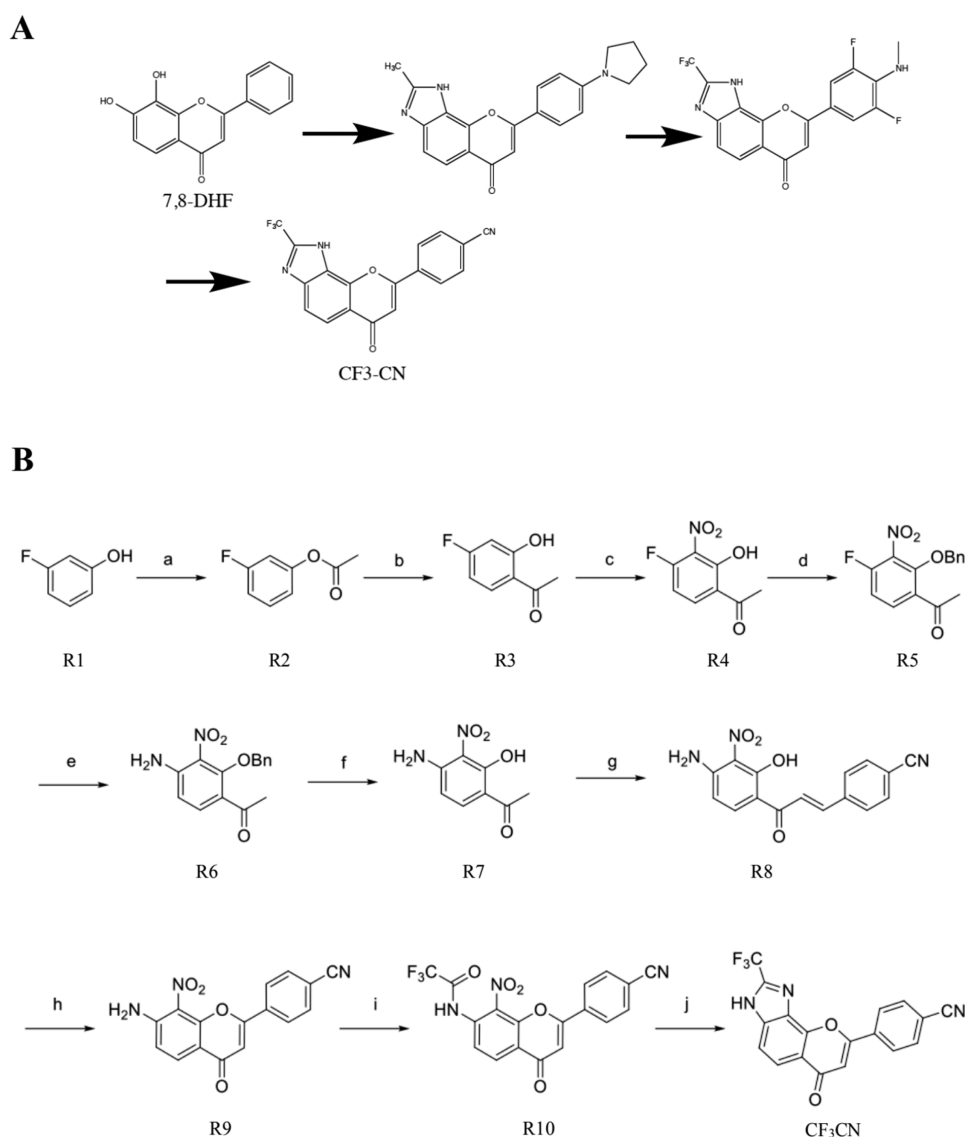
Figure 1. (A) CF$_3$CN, an optimized 7,8-DHF derivative as a bioisosteric TrkB receptor agonist. (B) The organic synthesis route for generating CF$_3$CN.

mitigates Tauopathies, rescuing cognitive dysfunctions.[3] Remarkably, Tau N368 is highly increased in AD patient brains and CSF, fitting with intensified Tau PET images in AD brains.[5] Thus, these studies demonstrate that delta-secretase might be an innovative drug target for treating AD. Accordingly, we performed a high throughput screening (HTS) and identified a promising small molecular inhibitor against delta-secretase. As expected, lead compound no. 11 potently blocks delta-secretase activation, revealing a potential therapeutic effect for treating AD.[6] Interestingly, delta-secretase also cleaves human α-Synuclein (α-Syn), a principal component in Parkinson's disease (PD)-associated Lewy bodies. Delta-secretase cuts α-Syn at N103 residue and augments its fibrillization and neurotoxicities. Inactivation of delta-secretase abolishes α-SNCA A53T-induced PD.[7]

Neurotrophins are a family of growth factors that regulate neuronal survival, development, and differentiation. There are four related proteins, including the brain-derived neurotrophic factor (BDNF), the nerve growth factor (NGF), neurotrophin-3 (NT-3), and neurotrophin-4 (NT-4/5). Neurotrophins trigger the trophic effects via the cognate Trk receptors.

Upon BDNF binding to TrkB receptors, it elicits the receptor dimerization and autophosphorylation on numerous tyrosine residues in the TrkB intracellular domain, leading to the activation of downstream signaling pathways including PI3K/Akt, Ras/Raf/MAPK, and PLC-γ1.[8] BDNF expression is reduced in the brains of different neurodegenerative diseases. For instance, BDNF mRNA and protein expression are decreased in multiple brain areas of AD post-mortem.[9,10] Neurons containing NFT do not contain BDNF immune-reactivity, whereas intense BDNF immune-reactivity neurons are devoid of tangles,[11] suggesting that BDNF may play a protective role against AD pathogenesis. Most recently, we have reported that BDNF-mediated Akt could directly phosphorylate delta-secretase on T322 residue and blocks its activation, sequestering its lysosomal residency. BDNF scarcity in neurodegenerative diseases leads to reduction of phosphorylation, cytoplasmic translocation and subsequent activation of delta-secretase, eliciting its autocleavage and pathological substrates truncation.[12] Exogenous application of BDNF has been documented to improve the learning and memory ability of a demented animal.[13] Studies in AD models show that
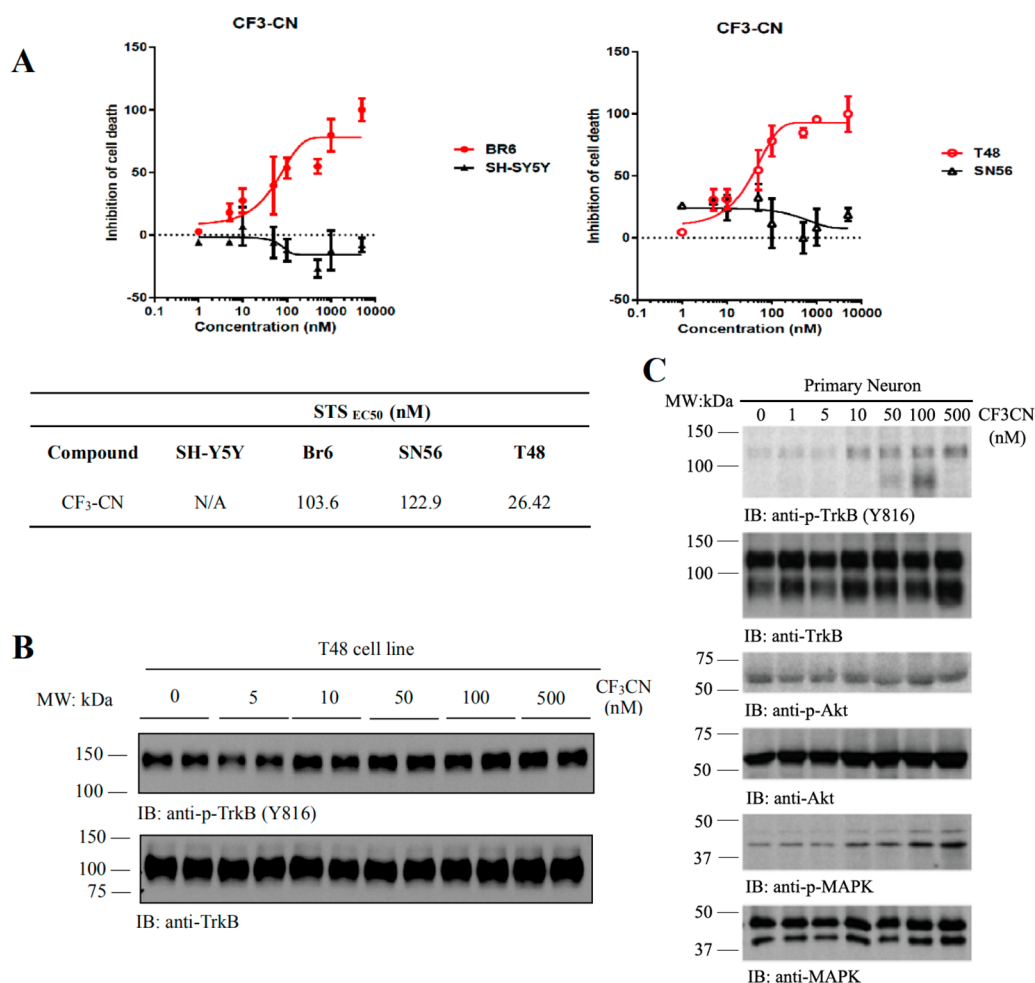
Figure 2. CF₃CN activates TrkB and its downstream signaling pathway in a dose-dependent manner. (A) CF₃CN protected T48 but not SN56 cells from STS-induced cell death. MTT assay was performed, and the EC₅₀ value was calculated on a nanomolar scale with Prism software. (B) CF₃CN activated TrkB and its downstream effectors in T48 cells dose-dependently. (C) CF₃CN activated TrkB dose-dependently in primary neurons.

BDNF plays a neuroprotective role against Aβ toxicity. Exogenous BDNF administration in primary neurons and *in vivo* reduces levels of murine Aβ.[14] Furthermore, application of BDNF *in vitro* dephosphorylates Tau protein via the TrkB signaling pathway,[15] indicating a neuroprotective role in the development of Tau pathology. Consequently, BDNF gene delivery has been shown as a novel potential therapeutic approach in diverse AD models.[16] Thus, preclinical evidence supports that BDNF administration might be a therapeutic agent for a variety of neurological disorders. However, the outcomes of several clinical trials using recombinant BDNF are disappointing. Presumably, this is due to poor delivery and the short *in vivo* half-life of BDNF.[17−19]

Employing a cell-based screening, we identified that 7,8-dihydroxyflavone (7,8-DHF) specifically binds to the extracellular domain of TrkB receptor and acts as a selective TrkB receptor agonist, which mimics the physiological functions of BDNF.[20,21] Oral administration of 7,8-DHF activates TrkB receptors in the brains and induces BDNF-like behavioral phenotypes in rodents in a TrkB-dependent way.[22−24] Several studies show that 7,8-DHF rescues learning and memory deficits in different AD animal models. 7,8-DHF inhibits the expression of BACE1 and reduces the levels of Aβ40 and Aβ42. Therefore, 7,8-DHF represents an innovative oral

bioactive therapeutic agent for treating AD.[25−29] Together, these studies support that 7,8-DHF shows prominent therapeutic efficacy toward AD through acting as a TrkB receptor agonist. Nevertheless, 7,8-DHF contains a catechol group that possesses intrinsic pharmacokinetic (PK) drawbacks including poor oral bioavailability and short half-life and suboptimal brain exposure. To alleviate these shortcomings, we conducted an extensive lead optimization campaign via medicinal chemistry modification,[21,24,30] and gained the structural insight critical for improving its druggability. In the study, we report that the newly optimized 7,8-DHF derivative CF₃CN robustly binds to the LCM/CC2 motif on TrkB ECD. It displays improved PK profiles including oral bioavailability and *in vivo* half-life. Oral administration of CF₃CN strongly activates TrkB receptors and its downstream signalings, leading to inhibition of delta-secretase by Akt phosphorylation. Noticeably, CF₃CN exhibits a tight PD/PK relationship and exerts promising therapeutic efficacy in 5xFAD mice in a dose-dependent manner.

■ RESULTS AND DISCUSSION

Organic Synthesis of 7,8-DHF Derivatives. Our previous structure−activity relationship (SAR) study shows that the catechol group in 7,8-DHF is critical for agonistic
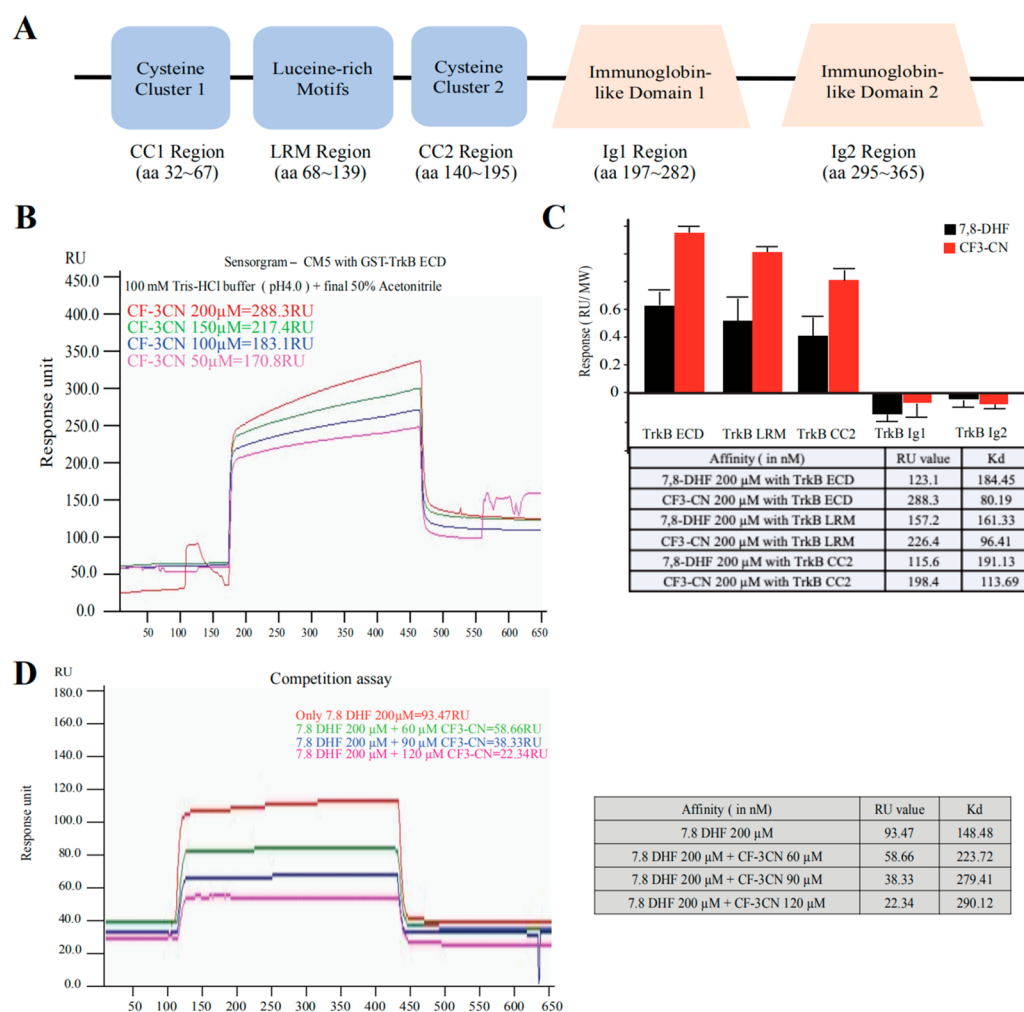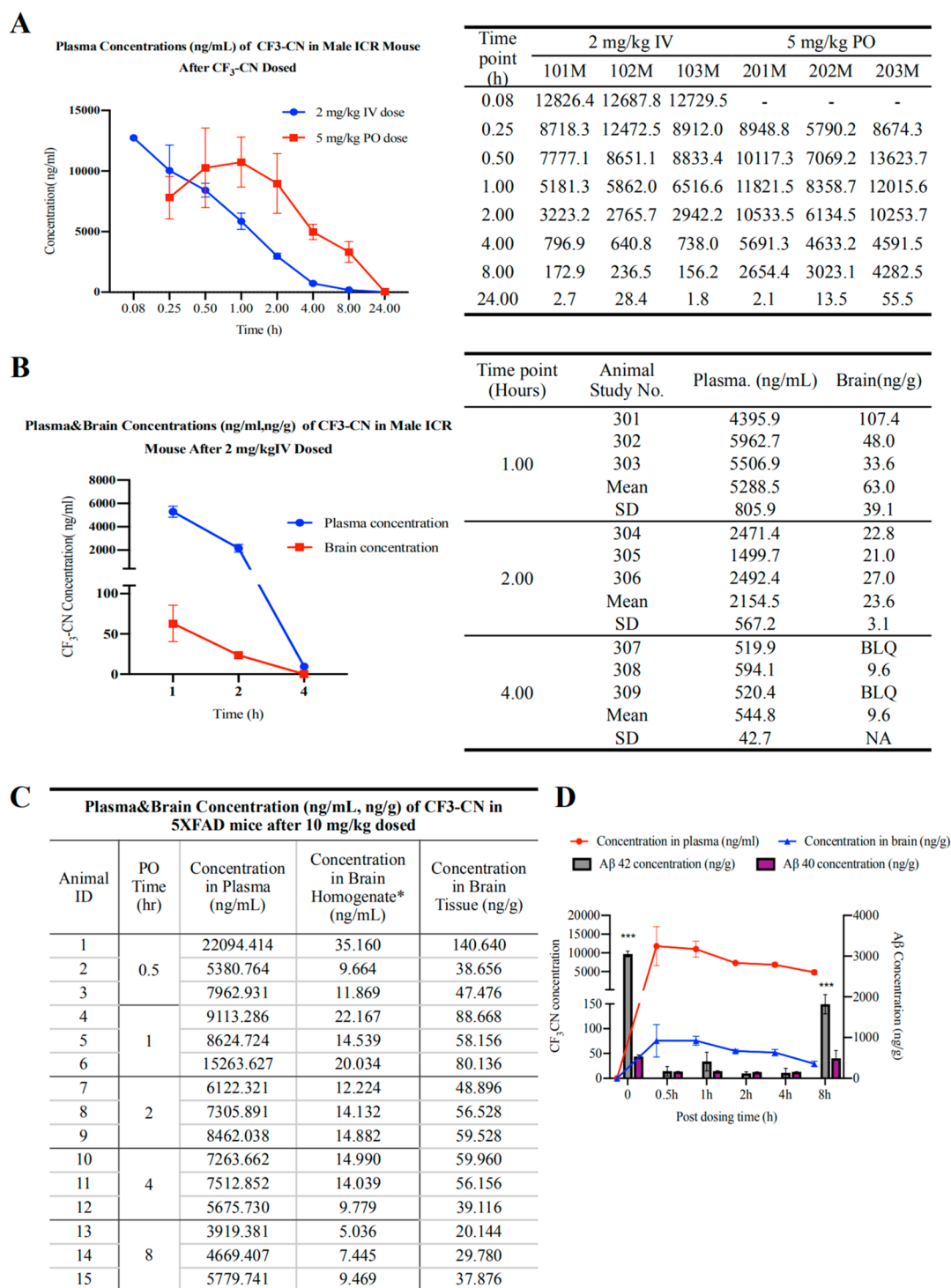
Figure 3. Synthetic derivatives bind to TrkB receptor in Biacore assay. (A) The schematic of human TrkB-ECD with an N-terminal GST tag. (B) Biacore assay of CF$_3$CN interaction with purified GST-TrkB ECD recombinant proteins. (C) Biacore binding assay. 7,8-DHF and CF$_3$CN bind to both TrkB LRM and the CC2 region. (D) CF$_3$−CN competition with 7,8-DHF binding to TrkB ECD in a dose-dependent manner.

activity. The synthetic imidazole derivatives via the bioisosteric strategy to modify the A ring in 7,8-DHF indicates that these compounds maintain the TrkB agonistic activity. However, the electron-donor groups in the B ring make the derivatives metabolically labile, though they enhance their agonistic potencies.[19,22] To alleviate the PK shortcomings and optimize the lead compound into an innovative preclinical candidate, we introduced the electron-withdrawing groups via medicinal chemistry approaches (Figure 1A) and synthesized dozens of derivatives and selected two of the optimal ones to present here. The organic synthesis routes for the final candidate CF$_3$CN is shown in Figure 1B.

CF$_3$CN Activates TrkB and Its Downstream Signaling Pathway in a Dose-Dependent Manner. One of the major physiological functions of BDNF/TrkB pathways is to promote neuronal survival. To determine whether the synthetic derivatives specifically activate TrkB and protect cells from apoptosis in a TrkB-dependent manner, we employed HA-TrkB stably transfected T48 cells, a murine cell line which originally was derived from basal forebrain SN56 cells that expressed negligible TrkB. Titration assay revealed that CF$_3$CN displayed a dose-dependent protection against staurosporine-induced apoptosis in T48 cells with EC$_{50}$ around 26.4 nM. By contrast, CF$_3$CN exhibited much weaker

protective effects in TrkB lacking SN56 cells. We conducted the similar experiments with the human TrkB receptor stably transfected dopaminergic cell line BR6, which was from SH-SY5Y cells that express negligible TrkB receptors and made the similar observations. Again, CF$_3$CN protected BR6 cells but not TrkB-deficient SH-SY5Y cells from STS-induced cell death (Figure 2A, upper panels). CF$_3$CN selectively protected BR6 but not SH-SY5Y cells with the IC$_{50}$ of 103 nM (Figure 2A, lower panel). Immunoblotting showed that CF$_3$CN gradually triggered p-TrkB activation in T48 cells as the concentrations progressively increased (Figure 2B). CF$_3$CN, like 7,8-DHF, robustly provoked TrkB activation in BR6 cells, which was barely visible in SH-SY5Y cells (data not shown). Both CF$_3$CN and 7,8-DHF exhibited the comparable protective profiles in BR6 cells via MTT assay, whereas neither of them displayed a demonstrable effect in TrkB-deficient SH-SY5Y cells (Figure 1B,C). To determine whether the synthetic derivatives also stimulate endogenous TrkB activation in primary neurons, we employed DIV13 primary cortical cultures and treated the neurons at the indicated doses for 15 min. CF$_3$CN displayed a dose-dependent effect in triggering TrkB activation, and the downstream p-Akt/p-MAPK consisted with p-TrkB activities (Figure 2C). Hence, CF$_3$CN activates p-TrkB and promotes cell survival in a TrkB-dependent manner.

A

Plasma Concentrations (ng/mL) of CF3-CN in Male ICR Mouse After CF₃-CN Dosed

Time point (h)	2 mg/kg IV			5 mg/kg PO		
	101M	102M	103M	201M	202M	203M
0.08	12826.4	12687.8	12729.5	-	-	-
0.25	8718.3	12472.5	8912.0	8948.8	5790.2	8674.3
0.50	7777.1	8651.1	8833.4	10117.3	7069.2	13623.7
1.00	5181.3	5862.0	6516.6	11821.5	8358.7	12015.6
2.00	3223.2	2765.7	2942.2	10533.5	6134.5	10253.7
4.00	796.9	640.8	738.0	5691.3	4633.2	4591.5
8.00	172.9	236.5	156.2	2654.4	3023.1	4282.5
24.00	2.7	28.4	1.8	2.1	13.5	55.5

B

Plasma&Brain Concentrations (ng/ml,ng/g) of CF3-CN in Male ICR Mouse After 2 mg/kgIV Dosed

Time point (Hours)	Animal Study No.	Plasma. (ng/mL)	Brain(ng/g)
	301	4395.9	107.4
	302	5962.7	48.0
1.00	303	5506.9	33.6
	Mean	5288.5	63.0
	SD	805.9	39.1
	304	2471.4	22.8
	305	1499.7	21.0
2.00	306	2492.4	27.0
	Mean	2154.5	23.6
	SD	567.2	3.1
	307	519.9	BLQ
	308	594.1	9.6
4.00	309	520.4	BLQ
	Mean	544.8	9.6
	SD	42.7	NA

C

Plasma&Brain Concentration (ng/mL, ng/g) of CF3-CN in 5XFAD mice after 10 mg/kg dosed

Animal ID	PO Time (hr)	Concentration in Plasma (ng/mL)	Concentration in Brain Homogenate* (ng/mL)	Concentration in Brain Tissue (ng/g)
1		22094.414	35.160	140.640
2	0.5	5380.764	9.664	38.656
3		7962.931	11.869	47.476
4		9113.286	22.167	88.668
5	1	8624.724	14.539	58.156
6		15263.627	20.034	80.136
7		6122.321	12.224	48.896
8	2	7305.891	14.132	56.528
9		8462.038	14.882	59.528
10		7263.662	14.990	59.960
11	4	7512.852	14.039	56.156
12		5675.730	9.779	39.116
13		3919.381	5.036	20.144
14	8	4669.407	7.445	29.780
15		5779.741	9.469	37.876

D

Figure 4. *In vivo* PK study of CF₃CN and PD/PK relationship. (A) *In vivo* PK study. ICR mice were given 2 mg/kg (i.v.) or 5 mg/kg (P.O.) CF3-CN, and blood samples were collected from all three mice at indicated time points. CF₃CN was quantitatively analyzed by LC-MS/MS. (B) CF₃CN brain exposure from intravenous administration of CF₃CN. Three ICR mice were given 2 mg/kg CF₃CN, which was dissolved in DMSO then resuspended in 95% methylcellulose (0.5%, wt/vol), and the final DMSO concentration is 5% (5% DMSO/95% methylcellulose, vol/vol). At indicated time points, blood samples were collected from all three mice. CF₃CN was quantitatively analyzed by LC-MS/MS. (C) Nine ICR mice were given 2 mg/kg CF₃CN, which was dissolved in DMSO then resuspended in 95% methylcellulose (0.5%, wt/vol), and the final DMSO concentration is 5% (5% DMSO/95% methylcellulose, vol/vol). At indicated time points, three mice per group were sacrificed, and serum and brain samples were collected. CF₃CN was quantitatively analyzed by LC-MS/MS. (D) Quantitative $A\beta40$ and 42 ELISA analysis in the brain lysates at different time points after oral administration of CF₃CN.

***In Vitro* ADMET Profilings of CF₃CN.** To assess the PK profiles for CF₃CN, we conducted a panel of *in vitro* ADMET assays. Based on *in vitro* plasma, hepatocyte, and liver microsomal stability assays, we found that CF₃CN is stable (Tables S1−S3) and brain permeable with good intestine absorption (Tables S4 and S5). Remarkably, CF₃CN is water-
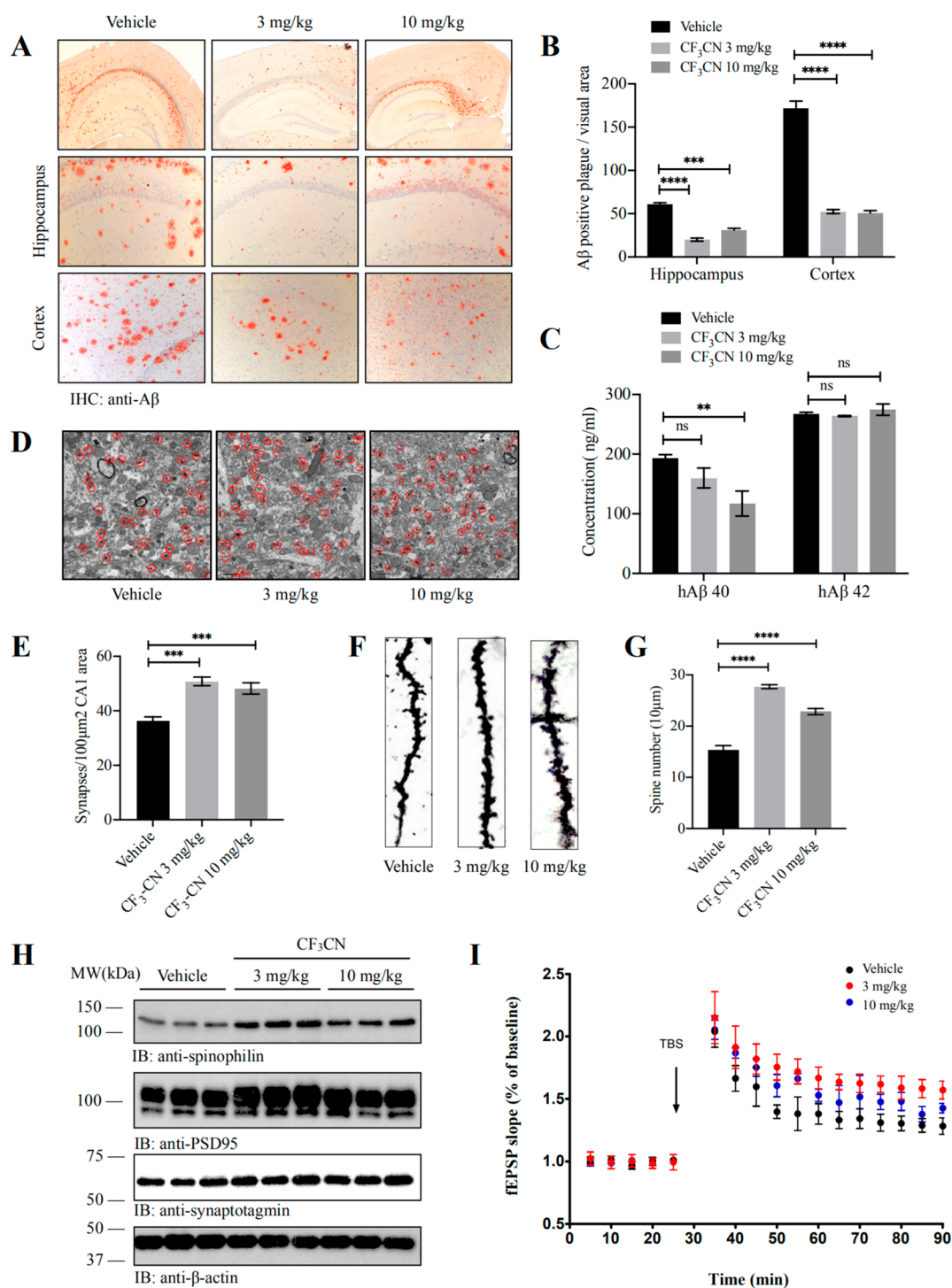
Figure 5. CF$_3$CN prevents the synaptic loss in the hippocampus of 5xFAD mice. (A) Immunohistochemistry of Aβ deposits in 5xFAD mice (scale bar, 100 μm). (B) Quantitative analysis of Aβ positive plaques in vehicle-treated and CF$_3$CN-treated 5xFAD mouse brains (n = 3, data are shown as mean $\pm$ SEM *** p < 0.001, **** p < 0.0001, two-way ANOVA). (C) Aβ42 and Aβ40 ELISA. CF3-CN did not reduce soluble Aβ40 or Aβ42 in the mouse brains (n = 3, data are shown as mean $\pm$ SEM ** p < 0.01, two-way ANOVA). (D) Representative electron microscopy pictures of the synaptic structures. Red circles indicate the synapses (scale bar, 1 μm). (E) Quantitative analysis of the synaptic density in vehicle and CF$_3$CN-treated 5xFAD mice. 5xFAD mice showed decreased synaptic density, which was reversed by CF$_3$CN (n = 5 in each group, data are shown as mean $\pm$ SEM *** p < 0.001, one-way ANOVA). (F) CF$_3$CN reversed the synaptic loss in 5xFAD mice. The dendritic spines from apical dendritic layer of the CA1 region were analyzed by Golgi staining (scale bar, 5 μm). (G) Quantitative analysis of the spine density. The decreased spine density in 5xFAD mice was reversed by CF$_3$CN treatment (n = 5 in each group, data are shown as mean $\pm$ SEM **** p < 0.0001, one-way ANOVA). (H) Immunoblotting analysis of synaptic markers in brain from mice treated with vehicle or CF$_3$CN. CF$_3$CN treatment increased the expression of synaptic markers in 5xFAD mice. (I) LTP of field excitatory postsynaptic potential (fEPSP) was induced by 3XTBS (theta-burst-stimulation) (four pulses at 100 Hz, repeated three times with a 200 ms interval). Shown traces are representative fEPSPs recorded at the time points 1 (vehicle-treated 5xFAD) and 2 (CF$_3$CN-treated 5xFAD mice) (n = 5 in each group. Data are presented as mean $\pm$ SEM. * p < 0.05, vehicle-treated vs CF$_3$CN-treated mice).

soluble (Table S6). The plasma protein binding assay showed that CF_3CN demonstrated robust plasma protein binding activities (Tables S7 and S8). The hERG inhibition assay revealed that CF_3CN did not bind to the potassium channel, suggesting that they do not possess any potential cardiovascular toxicity (Table S9). Together, *in vitro* ADMET data analysis reveals that CF_3CN is a promising lead compound.

CF_3CN Binds to LRM/CC2 Motifs on the TrkB Receptor Extracellular Domain. To determine whether the synthetic derivative CF_3CN directly binds to the TrkB extracellular domain (ECD), we coupled the recombinant proteins onto the biosensor chip and monitored the binding by the small molecule to the immobilized TrkB receptor using the standard biophysical protocol. As expected, CF_3CN exhibited a somewhat higher affinity to TrkB than 7,8-DHF; the Biacore binding assay showed that CF_3CN and 7,8-DHF interacted with GST-TrkB ECD with K_d values of 80.2 and 184.5 nM, respectively (Figure 3A−C). To map the exact domain on TrkB ECD (a.a. 1−428) implicated in associating with CF_3CN, we purified various truncated GST-tagged TrkB ECD recombinant proteins including LRM (leucine-rich motif, a.a. 37−111), CC2 (Cysteine Cluster 2, a.a. 112−176), Ig1 (a.a. 182−250), and Ig2 (a.a. 251−340). The proteins were purified by FPLC with the final concentrations around 0.5 mg/mL. The Biacore binding assay revealed that 7,8-DHF and CF_3CN strongly associated with the LRM domain, followed by the CC2 domain, and none of them associated with the Ig1 or Ig2 domains (Figure 3C; Figure S2). These findings are consistent with our previous reports that 7,8-DHF directly interacts with the TrkB ECD around LRM,[20,21] and BDNF interacts with the TrkB LRM domain as well.[31] Next, we conducted the binding competition assay of 7,8-DHF with TrkB ECD recombinant proteins in the presence of different concentrations of CF_3CN. The binding between 7,8-DHF and TrkB His-Sumo-LRM/CC2 recombinant proteins was reduced by gradually escalated CF_3CN in a dose-dependent manner (Figure 3D), suggesting that these two compounds occupy the same binding site on TrkB receptors and CF_3CN may possess a stronger binding affinity toward TrkB receptors.

***In Vivo* PK and Brain Exposure of CF_3CN and the PD/PK Relationship.** We tested the *in vivo* PK profiles of CF3-CN after dosing CF_3CN in three ICR mice at 2 mg/kg (intravenous, i.v.) and 5 mg/kg (by mouth, oral gavage), respectively. Blood samples were drawn from three animals after i.v. injection at each designated time point (5, 15, and 30 min, 1, 2, 4, 8, and 24 h), and CF_3CN concentrations in all plasma were measured by LC-MS/MS. The pharmacokinetic analysis was performed by using a noncompartmental method. CF_3CN was gradually decayed and barely detectable at 8 h (blue line) after i.v. injection. After a single oral administration of CF_3CN, the C_{max} and T_{max} values for CF_3CN were 11 268 ng/mL and 49.8 min, respectively. The mean value of area under the curve (AUC)(0-t) was 68 533.8 h ng/mL (Figure 4A). The mean oral bioavailability value for CF_3CN is approximately 136%. We also delivered an i.v. injection in 12 ICR mice at 2 mg/kg of CF_3CN for *in vivo* PK/BBB study and harvested brain samples from three mice after i.v. injection at 1, 2, and 4 h. The concentrations in the brain and plasma were determined. Following a single i.v. injection at 2 mg/kg, the C_{max} value for CF_3CN reached 12 747.9 ng/mL within 5 min in the plasma, while in the brains, the C_{max} and T_{max} were 63.3 ng/g and 1 h, respectively (Figure 4B). Hence, CF_3CN is brain permeable in mice.

To explore whether orally administered CF_3CN displays an optimal PD/PK relationship, we treated 2-month-old 5xFAD mice with a 10 mg/kg dose via oral gavage and sacrificed the mice and indicated time points. CF_3CN exhibited a time-dependent fluctuation in both the plasma and the brain. CF_3CN peaked in both tissues at 0.5 h and started to decay, and it was detectable in the brain at 8 h (Figure 4C). Quantification of $A\beta40$ and 42 peptides in the brains showed that $A\beta42$ was prominently reduced when CF_3CN entered the brain, and it bounced back at 8 h, when CF_3CN was substantially metabolized. Because the $A\beta40$ baseline in 5xFAD mice was very low as compared to that of $A\beta42$, $A\beta40$ concentrations were not altered much upon CF_3CN treatment (Figure 4D). Therefore, CF_3CN dose-dependently decreases $A\beta42$ in 5xFAD mouse brains, displaying a tight PD/PK relationship.

CF_3CN Alleviates $A\beta$ Deposition and Prevents Synaptic Loss in 5xFAD Mice. To determine whether oral administration of CF_3CN attenuates AD pathologies and synaptic loss in the brain, we treated 5xFAD mice daily with CF_3CN (3 or 10 mg/kg) or vehicle, beginning at 3 months of age. Three months after drug treatment, we detected the effect of CF_3CN treatment on $A\beta$ deposition through immunohistochemistry (IHC) staining the brain sections with anti-$A\beta$ antibody. Strikingly, the number of plaques and the plaque area fraction in both cortex and hippocampus areas were significantly decreased in CF_3CN-treated mice as compared with those of the vehicle group (Figure 5A,B). We further tested $A\beta$ deposition by immunofluorescent costaining with anti-$A\beta$ antibody and Thioflavin-S (ThS). The $A\beta$ deposition in both cortex and hippocampus regions was significantly lower in CF_3CN-treated mice than that in the vehicle group (Figure 3A,B). To verify whether CF_3CN inhibits $A\beta$ production, the concentrations of total $A\beta40$ and $A\beta42$ were quantified by ELISA. $A\beta40$ but not $A\beta42$ concentrations were reduced by CF_3CN in a dose-dependent manner (Figure 5C). Hence, these results suggest that chronic oral CF_3CN may decrease $A\beta$ production and prevent $A\beta$ deposition.

Synaptic loss is associated with cognitive impairment in the early phase of AD.[32] In 5xFAD mice model, significant synaptic loss and behavioral deficits are detected at 5 months old, while there is no detectable neuronal loss.[33] We assessed the densities of the synapse in the hippocampus CA1 area in the 5xFAD mice brains by electron microscopy (EM). Significant reduction in synaptic density was detected in 5xFAD mice. CF_3CN remarkably reversed the synaptic loss at both doses (Figure 5D,E). We quantified the density of dendritic spines of pyramidal neurons by Golgi staining. Interestingly, the spine densities were noticeably rescued by CF_3CN treatment as compared to vehicle control (Figure 5F,G). We further performed immunoblotting by using the presynaptic marker (synaptotagmin) and postsynaptic markers (PSD95 and spinophilin). CF_3CN treatment reversed the reduction of synaptic markers (Figure 5H), fitting with EM and Golgi staining observations. Electrophysiology analysis demonstrated that CF_3CN treatment increased LTP (long-term potentiation) (Figure 5I), fitting with the augmentation of synapses by CF_3CN. These results suggest that CF_3CN inhibits the synaptic loss and improves the synaptic plasticity in 5xFAD mice.

CF_3CN Activates Akt and Inhibits Delta-Secretase Activation and APP and Tau Proteolytic Cleavage in 5xFAD Mice. To determine whether CF_3CN administration
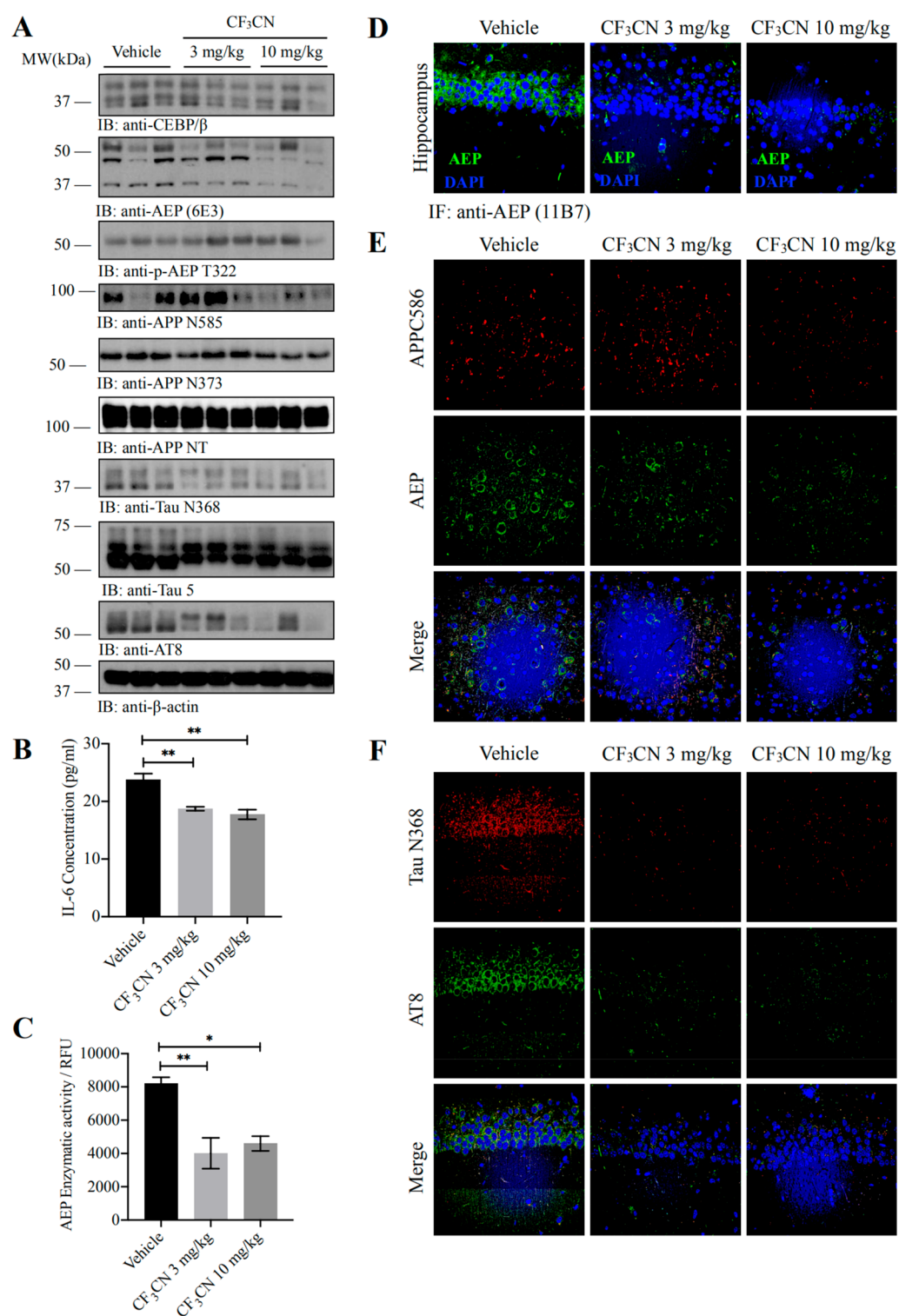
Figure 6. CF$_3$CN alleviates inflammation, inhibits AEP activation, and reduces the concentrations of AEP-derived APP fragments and Tau fragments. (A) Western blot showing the processing of APP and Tau by AEP. CF$_3$CN significantly inhibited AEP activation by phosphorylation of AEP T322, which attenuated Tau and APP cleavage. (B) Pro-inflammatory cytokine IL-6 was determined by ELISA kit. Chronic CF$_3$CN treatment significantly decreased the IL-6 production in mice brains compared with that of the age-related vehicle-treated mice ($n = 5$ in each group, data are shown as mean $\pm$ SEM **$p < 0.01$, one-way ANOVA). (C) AEP enzymatic activity analysis ($n = 5$ in each group, data are shown as mean $\pm$ SEM, *$P < 0.05$, **$P < 0.01$ compared with vehicle-treated mice brains, one-way ANOVA). (D) CF$_3$CN repressed AEP expression levels in 5xFAD mice. Immunofluorescence showing the presence of AEP positive cells in hippocampus of both vehicle- and CF$_3$CN-treated mice (scale bar, 50 μm). (E) CF$_3$CN inhibits AEP activation and reduces delta-secretase-derived APP fragments. Immunofluorescence staining of cortex from 5xFAD mice brains with AEP antibody (green), cleaved APP C586 fragment antibody (red), and DAPI (blue). (F) CF$_3$CN inhibits AEP activation and reduces delta-secretase-derived Tau fragments. Immunofluorescence staining of cortex from 5xFAD mice brain with cleaved Tau N368 fragment antibody (red), AT8 antibody (green), and DAPI (blue).
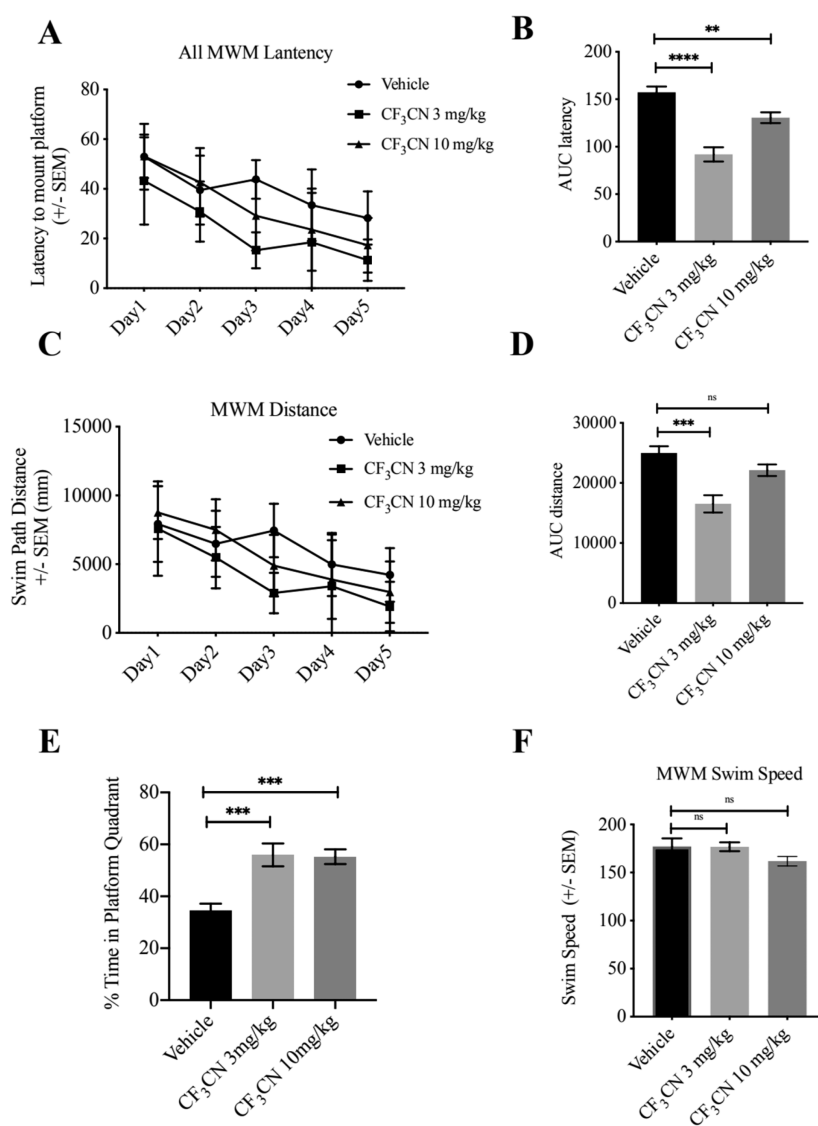
Figure 7. CF$_3$CN improves the spatial learning and memory of 5xFAD mice. CF$_3$CN improves the cognitive functions in 5xFAD mice. 5xFAD mice ($n = 8-10$/group) orally administrated with control vehicle or different doses CF$_3$CN were trained in the water maze over 5 days. Shown are the mean ± SEM latency to mount the escape platform (A), the area under the curve of latency (AUC latency) (B), the mean ± SEM Swim Path Distance (C), the Swim Speed (D), and the percentage of time spent in target quandrant (E), *$p < 0.05$, **$p < 0.01$, ***$p < 0.001$ compared to vehicle-treated 5xFAD mice, one-way ANOVA.

activates TrkB receptors in the brain, we conducted immunoblotting analysis with the brain lysates and found that the TrkB was notably activated in CF$_3$CN-treated mice as compared with that in the vehicle group. Quantitative analysis revealed that p-TrkB levels but not total TrkB levels were significantly elevated upon CF$_3$CN treatment. As expected, TrkB receptors were more prominently phosphorylated in CF$_3$CN-treated 5xFAD mice than those in the vehicle control, so were the downstream AKT and MAPK pathways (Figure S4A). This result was also confirmed in the hippocampus by immunofluorescence staining with anti-p-TrkB Y816 (Figure S4B). Currently, it remains unclear why the signals of p-TrkB/ p-Akt/p-MAPK at the dose of 10 mg/kg were slightly reduced compared to those at the dose of 3 mg/kg. p-TrkB and its downstream p-Akt/p-MAPK activation by CF$_3$CN indicate that the brain-penetrated CF$_3$CN engages its target and activates TrkB neurotrophic pathways in the brain.

Recently, we reported that delta-secretase (also called AEP) cleaves both APP and Tau, driving AD pathogenesis.[3,4] To determine whether CF$_3$CN affects delta-secretase's effect in AD pathologies, we performed immunoblotting and detected that mature and active delta-secretase was decreased by CF$_3$CN, correlating with the reduction of cleaved APP N373, N585 fragments, and the Tau N368 fragment in 5xFAD mouse brains. Notably, delta-secretase p-T322 activity was escalated by CF$_3$CN (Figure 6A). In alignment with the observation that C/EBPβ repression by CF$_3$CN, the downstream target of inflammatory factor IL-6 in 5xFAD mouse brains, was reduced by CF$_3$CN (Figure 6B). The enzymatic assay showed that AEP activities were repressed by CF$_3$CN. Fitting with these findings, immunofluorescence revealed that delta-secretase expression in the hippocampus was attenuated by CF$_3$CN (Figure 6C,D). To further assess APP proteolytic cleavage activity by delta-secretase, we conducted immunofluorescent costaining on 5xFAD brain sections with anti-APP

C586 and delta-secretase antibodies. APP C586 immunoreactive signals were strongly inhibited by CF$_3$CN, coupled with delta-secretase reduction (Figure 6E). Furthermore, Tau N368 and p-Tau (AT8) staining activities were also prominently diminished by CF$_3$CN (Figure 6F).

Chronic Oral Administration of CF$_3$CN Rescues the Learning and Memory Deficits in 5xFAD Mice. Morris water maze (MWM) tests were performed to test the hippocampus-dependent spatial memory of 5xFAD mice. The average latency (Figure 7A,B) and swim path length (Figure 7C,D) for each of the 5 acquisition days were calculated and plotted. The area under curve (AUC) of latency in vehicle-treated 5xFAD mice was larger than that in CF$_3$CN-treated mice, indicating that the learning deficit of 5xFAD mice was attenuated by CF$_3$CN treatment (Figure 7B). The swim path distance in 5xFAD mice showed a significant decrease at the dose of 3 mg/kg and reduction trend by CF$_3$CN at 10 mg/kg with no significant statistic differences (Figure 7D). The memory recall for the platform location was tested when the platform was removed, and the mice were allowed to search for 60 s. When compared to that of the vehicle group, CF$_3$CN-treated 5xFAD mice spent a significantly higher percentage of time in the target quadrant, revealing the rescue of spatial memory impairment (Figure 7E). All groups of mice displayed comparable swim speeds (Figure 7F). Together, our data strongly support that CF$_3$CN binds and activates TrkB receptors and the downstream neurotrophic signalings. It mimics the biological actions of BDNF and exerts the promising therapeutic efficacy toward neurodegenerative diseases including AD.

Employing reiterative organic synthesis of 7,8-DHF derivatives and cell-based TrkB-dependent survival assay and TrkB agonistic activity assays in primary neurons, we have successfully obtained a novel TrkB agonist CF$_3$CN that possesses a more robust binding affinity toward the TrkB receptor and a higher potency in activating TrkB in primary neurons and in mouse brains. Remarkably, this optimized preclinical candidate displays favorable *in vitro* ADMET and *in vivo* PK profiles. As a pharmacological agent for treating the CNS disorders, CF$_3$CN is orally bioactive and brain permeable, demonstrating exciting therapeutic efficacy in 5xFAD mice by strongly mitigating AD pathologies and effectively restoring cognitive functions. Notably, CF$_3$CN possesses improved druggable features with favorable *in vitro* ADMET characteristics and *in vivo* PK profiles. Chronic treatment (3 months) with a 10 times higher therapeutic dose of CF$_3$CN demonstrated that no adverse effects were identified in wild-type mice, supporting that this compound is chronically safe at least at a dose of 30 mg/kg (Figure S5). Clearly, the optimized lead compound CF$_3$CN meets the preclinical criteria of safety and efficacy and may be pushed into the development stage for pharmacologically treating the devastating neurodegenerative diseases.

Accumulating evidence shows that BDNF and TrkB levels are markedly decreased in AD. Furthermore, BDNF (Val66Met) polymorphism is associated with AD risk.[34,35] However, it is still unclear whether BDNF/TrkB reductions may be mechanistically involved in AD pathogenesis. Employing 5xFAD/TrkB ± mice, Devi and Ohno reported that TrkB reduction exacerbates Alzheimer's diseaselike signaling aberrations and memory deficits without affecting β-amyloidosis in 5xFAD mice.[36] Interestingly, it has been reported that BDNF induces a dephosphorylation of Tau protein through a PI3K

signaling mechanism.[15] BDNF promotes spine growth and Tau protein expression, and the knockdown of Tau significantly decreased the spine density in hippocampal neurons.[37] Both secreted and cellular BDNF levels are attenuated due to Tau hyperphosphorylation in primary neuronal cultures.[38] BDNF/TrkB signaling may play an important role in amyloidogenic processing. For example, Aβ production in cultured cells is reduced by BDNF treatment,[39] while it is facilitated by BDNF deprivation.[40] By examining AD-type neuropathology, levels of soluble Aβ and Tau protein or BDNF and TrkB levels correlate with dementia in the oldest subjects designated as oldest-old. Michalsi et al. found that soluble Aβ42 and BDNF levels, but not TrkB or soluble Tau levels, correlate with dementia in the oldest-old in post-mortem Brodmann's areas 7 and 9 (BA7 and BA9) in 4 groups of subjects >90 years old.[41] Here, we show that treatment with BDNF mimetic compound that selectively activates TrkB in the CNS substantially reduces Aβ production, suppressing senile plaque formation in 5xFAD mice. Mechanistically, we show that BDNF represses the amyloidogenic pathway via the blockade of delta-secretase, which is phosphorylated by CF$_3$CN-activated Akt in primary neurons and mouse brains (Figure 6). Accordingly, APP N585 and Tau N368 proteolytic cleavages by delta-secretase were conspicuously suppressed, leading to the reduction of Aβ and Tau pathologies (Figure 6). The BDNF/TrkB pathway promotes neuronal survival predominantly via PI3K/Akt signaling. BDNF reduction is associated with noticeable synaptic loss in AD.[42] Utilizing EM and Golgi staining, we demonstrate that CF$_3$CN robustly rescues synaptic loss and dendritic spine reduction in 5xFAD mice, resulting in LTP escalation in CF$_3$CN-treated 5xFAD mice (Figure 5). It is worth noting that CF$_3$CN treatment also diminishes delta-secretase expression levels in the hippocampus of 5xFAD (Figure 6). One of the potential mechanisms might be that CF$_3$CN activates the TrkB pathway and inhibits C/EBPβ, which is a crucial transcription factor for delta-secretase,[43] resulting in repression of *LGMN* mRNA transcription. As expected, we found that CF$_3$CN diminished C/EBPβ dose-dependently. Consequently, inflammatory cytokine IL-6, another downstream target of C/EBPβ, is reduced as well upon CF$_3$CN treatment (Figure 6).

In 5xFAD mouse brains, we observe that CF$_3$CN represses the delta-secretase upstream transcription factor C/EBPβ dose-dependently, leading to delta-secretase expression suppression. Accordingly, APP and Tau truncation by delta-secretase is reduced, fitting with delta-secretase enzymatic activities (Figure 6). Noticeably, delta-secretase P-T322 by Akt is upregulated upon CF$_3$CN treatment, in alignment with its effect in activation of p-TrkB/p-Akt/p-MAPK in 5xFAD (Figure S4). However, it remains unclear why TrkB neurotophic signaling activities are not escalated in 5xFAD mice by CF$_3$CN dose-dependently, though its inhibitory effect on delta-secretase and APP/Tau cleavage behaves in a dose-dependent manner (Figure 6). Cognitive behavioral tests show that CF$_3$CN rescues the cognitive defects in both doses, but it appears that 3 mg/kg is already saturated (Figure 7E). Presumably, the inconsistency might be due to the experimental variation. Because the animal experiments need a large number of age-matched young 5xFAD mice for chronic drug treatment, the *in vivo* experiments have to be conducted at different times to accumulate sufficient animals.

Most recently, we have reported that R13, a synthetic prodrug of 7,8-DHF, exhibits promising therapeutic efficacy

toward AD.[43] R13 optimizes 7,8-DHF's *in vivo* PK profiles. Chronic oral administration of R13 activates TrkB signaling and inhibits $A\beta$ deposition in 5xFAD mice, reducing the pathological cleavage of APP and Tau by delta-secretase. Moreover, R13 inhibits the synaptic loss and improves memory deficits in a dose-dependent manner, supporting that prodrug R13 is an optimal therapeutic agent for treating AD.[43] Here, we employ the bioisosteric strategy and perform a total organic synthesis based on our previous SAR knowledge about 7,8-DHF's crucial pharmacophore.[21,24] Now, we have substantially improved the lead compound's PK profiles. Utilizing an electron withdrawing group −CN to replace the electron donor −NR on the B ring, we successfully stabilize the optimized derivatives by decreasing the metabolism by P450s in liver microsomes and augmenting its half-life in the circulation system. By introduction of a hydrophobic and electron withdrawal CF3- group on the imidazole ring, we augment its brain exposure so that a demonstrable amount of CF_3CN could get access to its target TrkB receptors in the brain. The favorable safety profile and prominent therapeutic efficacy toward AD make us confident that CF_3CN is a promising preclinical candidate for further drug development. Our study demonstrates that CF_3CN represents a novel disease-modifying and neuroprotective pharmaceutical agent for the treatment of AD. Clearly, CF_3CN is not only useful for exploring the biological actions of BDNF/TrkB signaling but also providing a disease-modifying pharmacological intervention for clinical treatment of various neurological diseases including AD.

MATERIALS AND METHODS

Mice and Reagents. 5xFAD mice were obtained from Jackson lab and were bred in accordance with Emory Medical School guidelines. The 5xFAD mice received vehicle or CF_3CN dissolved in 5% DMSO/0.5% methylcellulose at a dose of 3 or 10 mg/kg/day. Mice were housed in AAALAC (American Association for Accreditation of Laboratory Animal Care)-Accredited facilities, and this study was approved by the institutional Animal Care and Use Committees at Emory University.

Anti-TrkB antibody was bought from Biovision (Milpitas, CA). Antiphospho-TrkB Y816 antibody was raised against [H]-CKLQNLAKASPV-pY-LDILG-[OH] (a.a. 806−822) (EM437 and EM438) as rabbit polyclonal antibody. Anti-synaptotagmin, anti-$A\beta$, and antitubulin were from Sigma-Aldrich (St Louis, MO). Anti-Akt, anti-p-Akt, anti-ERK, anti-p-ERK1/2, anti-synapsin I, anti-PSD95, and antispinophilin antibodies were bought from Cell Signaling (Boston, MA). The Histostain-SP kit and the $A\beta$ 1-42 ELISA kit was from Invitrogen (Grand Island, NY). All chemicals not included above were purchased from Sigma-Aldrich.

BIAcore X100 Binding Assay. 7,8-DHF solution was prepared in 20% DMSO + 80% 100 mM Tris−HCl (pH 4.0) (v/v). Purified TrkB ECD proteins (ECD, LRM, CC2, Ig1, Ig2) were reconstituted, respectively, to a concentration of 50 μg/mL in 10 mM sodium acetate (pH 4.0). The carboxylated dextran matrix on the sensor chip was activated by the injection of 60 μL of activation buffer prepared from the kit composed of 0.2 M N-ethyl-N'-(3-(dimethylamino)-propyl) carbodiimide and 0.05 M N-hydroxysuccimide in water. NaOH (75 μL of 50 mM) was employed for chip regeneration followed by applying the maximum volume of deionized water and running buffer (HEPES + EDTA + P20) (BIAcore, GE healthcare) according to the manual. The running time of the immobilization step was 180 s. The remaining binding sites on the sensor chip were blocked with 1 M ethanolamine, pH 8.5. To test the binding affinity between 7,8-DHF and different domains of TrkB ECD (LRM, LRM-CC2, Ig2, and CC1-CC2), 200 μM of 7,8-DHF solution was injected onto the derivatized sensor chip. Regeneration of the CM5 sensor

chip after each analysis cycle was performed by injecting 20 μL of 1.5 M glycine/HCl buffer pH 3.5 and 6 M guanidinium HCl pH 5.5. BIAevaluation software was used for K_d value analysis after the kinetics assay.

Primary Neuronal Cultures. All pregnant rats were purchased from the Jackson Laboratory. Primary cortical neurons were isolated from embryonic E18 Sprague−Dawley rats. Briefly, tissues were dissected, dissociated, and incubated with D-Hanks containing 0.25% trypsin for 5 min, centrifuged at $1000 \times g$ for 5 min after addition of the neuronal plating medium containing DMEM/F12 with 10% fetal bovine serum. Then, the cells were resuspended, about 5×10^5 cells were plated onto each well of 12-well plates. The neurons were cultured into a humidified incubator with 5% CO2 at 37 °C. The medium was changed to neurobasal medium supplemented with 2% B27 (maintenance medium) after 2−4 h. Neurons at 13 days *in vitro* (DIV 13) were treated with different doses of CF_3CN (0, 1, 5, 10, 50, 100, 500 nM) for 24 h. Then, the cells were harvested for Western blotting.

Cell Viability Assay. SH-SY5Y and Br6 cell lines were obtained from the laboratory of Garrett M. Brodeur's lab (Children's Hospital of Philadelphia). Mouse septal neuron × neuroblastoma hybrids SN56 cells were created by fusing N18TG2 neuroblastoma cells with murine (strain C57BL/6) neurons from postnatal day 21-septa. Our lab prepared stably transfected TrkB cell lines T48, which originally were derived from SN56 cells. Cell cytotoxicity was assessed *in vitro* using the 3-(4,5-dimethylthiazol-2-yl)-2,5-diphenyltetrazolium bromide (MTT) assay. Cells were treated with different doses of CF_3CN (0, 1, 5, 10, 50, 100, 500, 1000, 10 000 nM) for 24 h. After the incubation period, the MTT labeling reagent (final concentration 0.5 mg/mL) was added to each well and incubated for 2 h. The formazan product was dissolved with DMSO, and the absorbance of the formazan product was read using a microplate reader at a wavelength of 490 nm.

Golgi Staining. Mice brains were first fixed in 4% paraformaldehyde for 24 h and then soaked in 3% potassium bichromate buffer for 3 days in the dark. Then, the brains were transferred into 2% silver nitrate solution and incubated for 7 days in the dark. Slices were cut at 50 μm by Vibratome. Only spines that emerged perpendicular to the dendritic shaft were counted for quantification of spin density.

$A\beta$ Plaque Staining. Amyloid plaques were stained with Thioflavin-S. Free-floating brain slices were stained with 0.0125% Thioflavin-S for 5 min. The sections were washed in PBST for 15 min, three times. Then, the sections were covered with a glass cover using mounting solution.

$A\beta$ ELISA. To detect the $A\beta$ concentration in 5xFAD, the mice brains were homogenized in 8X mass of 5 M guanidine HCl/50 mM Tris HCl (pH 8.0) and incubated at room temperature for 3 h. The supernatant was analyzed by human $A\beta$40 and $A\beta$42 ELISA kit according to the manufacturer's instructions (KHB3481 and KHB3441, respectively, Invitrogen).

Morris Water Maze. Mice were trained in a round, water-filled tub (52 in. diameter) in an environment rich with extra maze cues. Each subject was given 3 trails/day for 5 consecutive days with a 15 min intertrial interval. The maximum trial length was 60 s, and if subjects did not reach the platform in the allotted time, they were manually guided to do it. Following the 5 days task acquisition, a probe trial was presented, during which time the platform was removed. All trials were analyzed for latency and swim speed by means of MazeScan (Clever Sys, Inc.).

Statistical Analysis. All data are expressed as mean ± SEM from three or more independent experiments, and the level of significance between two groups was assessed with Student's t test. For more than two groups, one-way ANOVA followed by the LSD post hoc test was applied. A value of $p < 0.05$ was considered to be statistically significant.

Organic Synthesis of CF_3CN. *General.* All reagents were commercial and were used without further purification. Silica gel TLC plates (Qing Dao Marine Chemical Factory, Qingdao, China) were used to monitor the progression of the reactions. Flash column chromatography was performed using silica gel (300−400 mesh size,

Qing Dao Marine Chemical Factory, Qingdao, China). All reactions were monitored by thin-layer chromatography (TLC) and LCMS. ^{1}H NMR spectra were recorded on a Bruker Avance III 400 MHz and Varian Mercury Plus 400 MHz, and TMS was used as an internal standard. LCMS was taken on a quadrupole mass spectrometer on an Agilent LC/MSD 1200 Series (column: BP-C18 (50 mm × 4.6 mm, 5 μm) operating in ES (+) or (−) ionization modes; T = 30 °C; flow rate = 1.5 mL/min; detected wavelength = 254 nm).

Reagents and conditions: (a) Ac_2O, pyridine, DCM, 0 °C, 3 h; (b) $AlCl_3$, 180 °C, 3 h; (c) H_2SO_4, HNO_3, 0 °C, 30 min; (d) BnBr, K_2CO_3, ACN, 70 °C, overnight; (e) DMSO, $NH_3\cdot H_2O$, 50 °C, 2 h; (f) DCM, BBr_3, rt, 2 h; (g) 4-formylbenzonitrile, DMF, NaH, rt, 5 h; (h) DMSO, I_2, 130 °C, 1 h; (i) DMF, TFAA, rt, 3 h; (j) MeOH, Fe, 50 °C, overnight.

Preparation of CF_3CN (Figure 1B). R 2. To a solution of R **1** (200 g, 1.57 mol) in DCM (2 L), pyridine (155 g, 1.96 mol) and Ac_2O (200 g, 1.96 mol) were added at 0 °C. The mixture was stirred at 0 °C for 3 h. Ice−water (2 L) was added. The mixture was extracted with DCM (1000 mL × 2), and the combined organic layer was washed with brine, dried over Na_2SO_4, and evaporated in a vacuum to give R **2** (190 g, yield 69%) as a red oil. ^{1}H NMR ($CDCl_3$, 400 MHz): δ (ppm) 2.29 (s, 3H), 6.84−6.96 (m, 3H), 7.29−7.37 (m, 1H).

R 3. A mixture of R **2** (190 g, 1.23 mol) and $AlCl_3$ (295 g, 2.22 mol) was stirred at 180 °C for 3 h under N_2 atmosphere. The mixture was cooled to room temperature and cold water (1 L) was added, it was extracted with DCM (1000 mL × 2). The combined organic layer was washed with brine (1000 mL), dried over Na_2SO_4, and evaporated in vacuum to give the crude product which was purified by column chromatography on silica gel to give R **3** (104 g, yield 67.5%) as a white solid. ^{1}H NMR ($CDCl_3$, 400 MHz): δ (ppm) 2.62 (s, 3H), 6.63−6.69 (m, 2H), 7.73−7.79 (m, 1H), 12.60 (s, 1H).

R 4. To a solution of concentrated (conc.) H_2SO_4 (400 mL), R **3** (100 g, 0.65 mmol) was added at 0 °C. The conc. HNO_3 (66 mL) was added to the mixture dropwise at 0 °C for 30 min. After addition, ice−water (2 L) was added. The mixture was extracted with EtOAc (500 mL × 2). The combined organic layer was washed with brine (1000 mL), dried over Na_2SO_4, and evaporated in *vacuum* to give the residue which was purified by column chromatography on silica gel (eluent: petroleum ether/ethyl acetate = 10/1−3/1) to give R **7** (45 g, yield 35%) as a yellow solid. ^{1}H NMR ($CDCl_3$, 400 MHz): δ (ppm) 2.67 (s, 3H), 6.77−6.83 (t, J = 9.0 Hz, 1H), 7.90−7.95 (dd, J = 9.0, 6.3 Hz, 1H), 13.30 (s, 1H).

R 5. A solution of R **4** (10 g, 0.05 mol), K_2CO_3 (13.8 g, 0.1 mol), and BnBr (9.35 g, 0.055 mol) in ACN (100 mL) was stirred at 70 °C overnight. The mixture was concentrated and then diluted with water (100 mL). The mixture was extracted with EtOAc (100 mL × 2). The combined organic layer was washed with water (200 mL) and brine (200 mL), dried over Na_2SO_4, and evaporated in vacuum to give R **5** (6 g, yield 41.4%) as yellow solid. ^{1}H NMR ($CDCl_3$, 400 MHz): δ (ppm) 2.56 (s, 3H), 5.06 (s, 2H), 7.08−7.11 (t, J = 8.7 Hz, 1H), 7.36−7.41 (m, 5H), 7.77−7.82 (dd, J = 9.0, 6.3 Hz, 1H).

R 6. To a solution of R **5** (10 g, 34.6 mmol) in DMSO (50 mL), $NH_3\cdot H_2O$ was added dropwise at rt. The reaction was stirred at 50 °C for 1 h. The mixture was poured into water (60 mL) and extracted with EtOAc (50 mL × 2). The combined organic layer was washed with water (100 mL × 3) and brine (100 mL × 2), dried over Na_2SO_4, and filtered. The filtrate was concentrated to give crude R **6** (7.2 g, yield 83.6%) as a red oil. ^{1}H NMR ($CDCl_3$, 400 MHz): δ (ppm) 2.52 (s, 3H), 5.00 (s, 2H), 5.35 (s, 2H), 6.58−6.60 (d, J = 8.8 Hz, 1H), 7.37−7.44 (m, 5H). 7.69−7.70 (d, J = 8.8 Hz, 1H).

R 7. To the solution of R **6** (8 g, 28 mmol) in DCM (80 mL), boron tribromide was added dropwise at −78 °C. The reaction was stirred at rt for 2 h. MeOH was added dropwise to the above mixture at 0 °C. The reaction was diluted with water (100 mL) and extracted with EtOAc (50 mL × 2). The organic layer was washed with water (100 mL) and brine (100 mL), dried over Na_2SO_4, and concentrated in vacuum to give crude product which was triturated with EtOAc to give R **7** (3 g, yield 37%) as a yellow solid. ^{1}H NMR ($CDCl_3$, 400 MHz): δ (ppm) 2.70 (s, 3H), 8.01−8.04 (d, J = 12.2 Hz, 2H).

R 8. To a solution of compound **7** (3 g, 15.3 mmol) in DMF (30 mL), NaH (1.8 g, 45.9 mmol) was added batchwise at 0 °C, and the mixture was stirred at room temperature for 0.5 h. The solution of 4-formylbenzonitrile (3.93 g, 30 mmol) in DMF (5 mL) was added to the above solution dropwise at 0 °C. The mixture was stirred at r.t for 3 h. The mixture was quenched with water and filtered, the filtrate cake was dried in *vacuum* to give R **8** (2.2 g, yield 49%) as a yellow solid. ^{1}H NMR ($CDCl_3$, 400 MHz): δ (ppm) 6.49−6.52 (d, J = 9.2 Hz, 1H), 7.68 (s, 2H), 7.82−7.86 (d, J = 15.2 Hz, 1H), 7.93−7.95 (d, J = 8 Hz, 2H), 8.07−8.12 (m, 3H), 8.23−8.25 (d, J = 9.2 Hz, 1H).

R 9. To a solution of compound **8** (2.2 g, 7.12 mmol) in DMSO (10 mL), I_2 (270 mg, 1.07 mmol) was added in one batch. The mixture was stirred at 130 °C for 1 h. The mixture was cooled to room temperature and quenched with ice−water (100 mL). The precipitate was filtered, and the filtrate cake was triturated with MeOH (10 mL × 2) to give R **9** (1.1 g, yield 50%) as a yellow solid. ^{1}H NMR ($CDCl_3$, 400 MHz): δ (ppm) 6.99−7.02 (d, J = 9.2 Hz, 1H), 7.23 (s, 1H), 7.87−7.90 (d, J = 9.2 Hz, 2H), 8.07−8.09 (d, J = 8.8 Hz, 2H), 8.21−8.23 (d, J = 8.8 Hz, 2H).

R 10. To a mixture of compound **9** (500 mg, 1.63 mmol) in pyridine (10 mL), TFAA (1.03 g, 4.89 mmol) was added dropwise at 0 °C, and the mixture was stirred at room temperature for 2 h. The mixture was diluted with water (10 mL) and extracted with EtOAc (10 mL × 2). The organic layer was washed with HCl (0.5 M, 10 mL) and brine (100 mL), dried over Na_2SO_4, and concentrated in vacuum to give R **10** (405 mg, yield 66.7%) as a yellow solid. ^{1}H NMR ($CDCl_3$, 400 MHz): δ (ppm) 7.38 (s, 1H), 7.74−7.76 (d, J = 8.4 Hz, 1H), 8.09−8.17 (m, 4H), 8.28−8.30 (d, J = 8.8 Hz, 1H).

CF_3CN. To a solution of R **10** (405 mg, 1.09 mmol) and Fe (304 mg, 5.4 mmol) in MeOH (10 mL), HAc (5 mL) was added in portions. The mixture was stirred at 50 °C for 2 h. The mixture was filtered; the filtrate was poured into water (20 mL) and extracted with EtOAc (20 mL × 2). The combined organic layer was washed with water (20 mL × 2) and brine (20 mL x 2), dried over Na_2SO_4, and filtered. The filtrate was concentrated to give crude product which was purified by prep-HPLC to give CF_3CN (300 mg, yield 77.9%) as a yellow solid. ^{1}H NMR (DMSO-d_6, 400 MHz): δ (ppm) 7.33 (s, 1H), 7.75−7.77 (d, J = 8.8 Hz, 1H), 7.98−8.00 (d, J = 8.8 Hz, 1H), 8.10−8.12 (d, J = 8.4 Hz, 2H), 8.37−8.39 (d, J = 7.6 Hz, 2H); purity > 98% at 220 nm, MS (ESI) m/z = 356.1 $[M + H]^+$.

■ ASSOCIATED CONTENT

Supporting Information

The Supporting Information is available free of charge at https://pubs.acs.org/doi/10.1021/acschemneuro.1c00181.

> CF_3CN selectively protects human TrkB stably transfected BR6 cells but not SH-SY5Y cells, CF_3CN selectively binds to TrkB LRM and CC2 domains, CF_3CN decreases Aβ plaque deposition in 5xFAD mice, CF_3CN elicits TrkB and downstream signaling activation in 5xFAD mice, 12 weeks treatment with CF_3CN demonstrates no toxic effect on tissue and blood, plasma stability half-life data summary, microsomal intrinsic clearance data summary, heptatocyte stability half-life data summary, Caco-2 permeability data summary, BBB-PAMPA permeability data summary, turbidimetric solubility screen data summary, human plasma protein binding data summary, mouse plasma protein binding data summary, and percent reduction of hERG current (PDF)

■ AUTHOR INFORMATION

Corresponding Author

Keqiang Ye − *Department of Pathology and Laboratory Medicine, Emory University School of Medicine, Atlanta,*

Georgia 30322, United States; orcid.org/0000-0002-7657-8154; Email: kye@emory.edu

Authors

Chun Chen − Department of Pathology and Laboratory Medicine, Emory University School of Medicine, Atlanta, Georgia 30322, United States

Eun H. Ahn − Department of Pathology and Laboratory Medicine, Emory University School of Medicine, Atlanta, Georgia 30322, United States

Xia Liu − Department of Pathology and Laboratory Medicine, Emory University School of Medicine, Atlanta, Georgia 30322, United States

Zhi-Hao Wang − Department of Pathology and Laboratory Medicine, Emory University School of Medicine, Atlanta, Georgia 30322, United States

Shilin Luo − Department of Pathology and Laboratory Medicine, Emory University School of Medicine, Atlanta, Georgia 30322, United States

Jianming Liao − Department of Pathology and Laboratory Medicine, Emory University School of Medicine, Atlanta, Georgia 30322, United States; Department of Neurosurgery, Renmin Hospital, Wuhan University, Wuhan, Hubei Province 430060, China; orcid.org/0000-0002-6196-0510

Complete contact information is available at:
https://pubs.acs.org/10.1021/acschemneuro.1c00181

Author Contributions

K.Y. conceived the project, designed the experiments, analyzed the data, and wrote the manuscript. C.C. and E.H.A. designed and performed most of the experiments and analyzed the data. Z.-H.W., S.L., J.L., and X.L. prepared primary neurons and assisted with *in vivo* and *in vitro* experiments.

Notes

The authors declare no competing financial interest.

■ REFERENCES

(1) Mattson, M. P. (2004) Pathways towards and away from Alzheimer's disease. *Nature* 430, 631−639.

(2) Vassar, R., Kovacs, D. M., Yan, R., and Wong, P. C. (2009) The beta-secretase enzyme BACE in health and Alzheimer's disease: regulation, cell biology, function, and therapeutic potential. *J. Neurosci.* 29, 12787−12794.

(3) Zhang, Z., Song, M., Liu, X., Kang, S. S., Kwon, I.-S., Duong, D. M., Seyfried, N. T., Hu, W. T., Liu, Z., Wang, J.-Z., Cheng, L., Sun, Y. E., Yu, S. P., Levey, A. I., and Ye, K. (2014) Cleavage of tau by asparagine endopeptidase mediates the neurofibrillary pathology in Alzheimer's disease. *Nat. Med.* 20, 1254−1262.

(4) Zhang, Z., Song, M., Liu, X., Su Kang, S., Duong, D. M., Seyfried, N. T., Cao, X., Cheng, L., Sun, Y. E., Ping Yu, S., Jia, J., Levey, A. I., and Ye, K. (2015) Delta-secretase cleaves amyloid precursor protein and regulates the pathogenesis in Alzheimer's disease. *Nat. Commun.* 6, 8762.

(5) Leuzy, A., Cicognola, C., Chiotis, K., Saint-Aubert, L., Lemoine, L., Andreasen, N., Zetterberg, H., Ye, K., Blennow, K., Höglund, K., and Nordberg, A. (2019) Longitudinal tau and metabolic PET imaging in relation to novel CSF tau measures in Alzheimer's disease. *Eur. J. Nucl. Med. Mol. Imaging* 46, 1152−1163.

(6) Zhang, Z., Obianyo, O., Dall, E., Du, Y., Fu, H., Liu, X., Kang, S. S., Song, M., Yu, S.-P., Cabrele, C., Schubert, M., Li, X., Wang, J.-Z., Brandstetter, H., and Ye, K. (2017) Inhibition of delta-secretase improves cognitive functions in mouse models of Alzheimer's disease. *Nat. Commun.* 8, 14740.

(7) Zhang, Z., Kang, S. S., Liu, X., Ahn, E. H., Zhang, Z., He, L., Iuvone, P. M., Duong, D. M., Seyfried, N. T., Benskey, M. J., Manfredsson, F. P., Jin, L., Sun, Y. E., Wang, J.-Z., and Ye, K. (2017) Asparagine endopeptidase cleaves α-synuclein and mediates pathologic activities in Parkinson's disease. *Nat. Struct. Mol. Biol.* 24, 632−642.

(8) Huang, E. J., and Reichardt, L. F. (2003) Trk receptors: roles in neuronal signal transduction. *Annu. Rev. Biochem.* 72, 609−642.

(9) Murer, M. G., Yan, Q., and Raisman-Vozari, R. (2001) Brain-derived neurotrophic factor in the control human brain, and in Alzheimer's disease and Parkinson's disease. *Prog. Neurobiol.* 63, 71−124.

(10) Peng, S., Garzon, D. J., Marchese, M., Klein, W., Ginsberg, S. D., Francis, B. M., Mount, H. T., Mufson, E. J., Salehi, A., and Fahnestock, M. (2009) Decreased brain-derived neurotrophic factor depends on amyloid aggregation state in transgenic mouse models of Alzheimer's disease. *J. Neurosci.* 29, 9321−9329.

(11) Murer, M. G., Boissiere, F., Yan, Q., Hunot, S., Villares, J., Faucheux, B., Agid, Y., Hirsch, E., and Raisman-Vozari, R. (1999) An immunohistochemical study of the distribution of brain-derived neurotrophic factor in the adult human brain, with particular reference to Alzheimer's disease. *Neuroscience* 88, 1015−1032.

(12) Wang, Z. H., Wu, W., Kang, S. S., Liu, X., Wu, Z., Peng, J., Yu, S. P., Manfredsson, F. P., Sandoval, I. M., Liu, X., Wang, J. Z., and Ye, K. (2018) BDNF inhibits neurodegenerative disease-associated asparaginyl endopeptidase activity via phosphorylation by AKT. *JCI insight* 3, 1 DOI: 10.1172/jci.insight.99007.

(13) Ando, S., Kobayashi, S., Waki, H., Kon, K., Fukui, F., Tadenuma, T., Iwamoto, M., Takeda, Y., Izumiyama, N., Watanabe, K., and Nakamura, H. (2002) Animal model of dementia induced by entorhinal synaptic damage and partial restoration of cognitive deficits by BDNF and carnitine. *J. Neurosci. Res.* 70, 519−527.

(14) Arancibia, S., Silhol, M., Moulière, F., Meffre, J., Höllinger, I., Maurice, T., and Tapia-Arancibia, L. (2008) Protective effect of BDNF against beta-amyloid induced neurotoxicity in vitro and in vivo in rats. *Neurobiol. Dis.* 31, 316−326.

(15) Elliott, E., Atlas, R., Lange, A., and Ginzburg, I. (2005) Brain-derived neurotrophic factor induces a rapid dephosphorylation of tau protein through a PI-3 Kinase signalling mechanism. *European journal of neuroscience* 22, 1081−1089.

(16) Nagahara, A. H., Merrill, D. A., Coppola, G., Tsukada, S., Schroeder, B. E., Shaked, G. M., Wang, L., Blesch, A., Kim, A., Conner, J. M., Rockenstein, E., Chao, M. V., Koo, E. H., Geschwind, D., Masliah, E., Chiba, A. A., and Tuszynski, M. H. (2009) Neuroprotective effects of brain-derived neurotrophic factor in rodent and primate models of Alzheimer's disease. *Nat. Med.* 15, 331−337.

(17) Ochs, G., Penn, R. D., York, M., Giess, R., Beck, M., Tonn, J., Haigh, J., Malta, E., Traub, M., Sendtner, M., and Toyka, K. V. (2000) A phase I/II trial of recombinant methionyl human brain derived neurotrophic factor administered by intrathecal infusion to patients with amyotrophic lateral sclerosis. *Amyotrophic Lateral Scler. Other Mot. Neuron Disord.* 1, 201−206.

(18) Angelova, A., and Angelov, B. (2017) Dual and multi-drug delivery nanoparticles towards neuronal survival and synaptic repair. *Neural Regener. Res.* 12, 886−889.

(19) Guerzoni, L. P., Nicolas, V., and Angelova, A. (2017) In Vitro Modulation of TrkB Receptor Signaling upon Sequential Delivery of Curcumin-DHA Loaded Carriers Towards Promoting Neuronal Survival. *Pharm. Res.* 34, 492−505.

(20) Jang, S. W., Liu, X., Yepes, M., Shepherd, K. R., Miller, G. W., Liu, Y., Wilson, W. D., Xiao, G., Blanchi, B., Sun, Y. E., and Ye, K. (2010) A selective TrkB agonist with potent neurotrophic activities by 7,8-dihydroxyflavone. *Proc. Natl. Acad. Sci. U. S. A. 107*, 2687−2692.

(21) Liu, X., Obianyo, O., Chan, C. B., Huang, J., Xue, S., Yang, J. J., Zeng, F., Goodman, M., and Ye, K. (2014) Biochemical and biophysical investigation of the brain-derived neurotrophic factor mimetic 7,8-dihydroxyflavone in the binding and activation of the TrkB receptor, *The. J. Biol. Chem. 289*, 27571−27584.

(22) Choi, D. C., Maguschak, K. A., Ye, K., Jang, S. W., Myers, K. M., and Ressler, K. J. (2010) Prelimbic cortical BDNF is required for memory of learned fear but not extinction or innate fear. *Proc. Natl. Acad. Sci. U. S. A. 107*, 2675−2680.

(23) Andero, R., Heldt, S. A., Ye, K., Liu, X., Armario, A., and Ressler, K. J. (2011) Effect of 7,8-dihydroxyflavone, a small-molecule TrkB agonist, on emotional learning. *Am. J. Psychiatry 168*, 163−172.

(24) Liu, X., Chan, C. B., Jang, S. W., Pradoldej, S., Huang, J., He, K., Phun, L. H., France, S., Xiao, G., Jia, Y., Luo, H. R., and Ye, K. (2010) A synthetic 7,8-dihydroxyflavone derivative promotes neurogenesis and exhibits potent antidepressant effect. *J. Med. Chem. 53*, 8274−8286.

(25) Devi, L., and Ohno, M. (2012) 7,8-dihydroxyflavone, a small-molecule TrkB agonist, reverses memory deficits and BACE1 elevation in a mouse model of Alzheimer's disease. *Neuropsychopharmacology 37*, 434−444.

(26) Zhang, Z., Liu, X., Schroeder, J. P., Chan, C. B., Song, M., Yu, S. P., Weinshenker, D., and Ye, K. (2014) 7,8-dihydroxyflavone prevents synaptic loss and memory deficits in a mouse model of Alzheimer's disease. *Neuropsychopharmacology 39*, 638−650.

(27) Castello, N. A., Nguyen, M. H., Tran, J. D., Cheng, D., Green, K. N., and LaFerla, F. M. (2014) 7,8-Dihydroxyflavone, a small molecule TrkB agonist, improves spatial memory and increases thin spine density in a mouse model of Alzheimer disease-like neuronal loss. *PLoS One 9*, e91453.

(28) Gao, L., Tian, M., Zhao, H. Y., Xu, Q. Q., Huang, Y. M., Si, Q. C., Tian, Q., Wu, Q. M., Hu, X. M., Sun, L. B., McClintock, S. M., and Zeng, Y. (2016) TrkB activation by 7, 8-dihydroxyflavone increases synapse AMPA subunits and ameliorates spatial memory deficits in a mouse model of Alzheimer's disease. *J. Neurochem. 136*, 620−636.

(29) Aytan, N., Choi, J. K., Carreras, I., Crabtree, L., Nguyen, B., Lehar, M., Blusztajn, J. K., Jenkins, B. G., and Dedeoglu, A. (2018) Protective effects of 7,8-dihydroxyflavone on neuropathological and neurochemical changes in a mouse model of Alzheimer's disease. *Eur. J. Pharmacol. 828*, 9−17.

(30) Obianyo, O., and Ye, K. (2013) Novel small molecule activators of the Trk family of receptor tyrosine kinases. *Biochim. Biophys. Acta, Proteins Proteomics 1834*, 2213−2218.

(31) Windisch, J. M., Auer, B., Marksteiner, R., Lang, M. E., and Schneider, R. (1995) Specific neurotrophin binding to leucine-rich motif peptides of TrkA and TrkB. *FEBS Lett. 374*, 125−129.

(32) Shankar, G. M., and Walsh, D. M. (2009) Alzheimer's disease: synaptic dysfunction and Abeta. *Mol. Neurodegener. 4*, 48.

(33) Hongpaisan, J., Sun, M. K., and Alkon, D. L. (2011) PKC epsilon activation prevents synaptic loss, Abeta elevation, and cognitive deficits in Alzheimer's disease transgenic mice. *J. Neurosci. 31*, 630−643.

(34) Lim, Y. Y., Villemagne, V. L., Laws, S. M., Ames, D., Pietrzak, R. H., Ellis, K. A., Harrington, K. D., Bourgeat, P., Salvado, O., Darby, D., Snyder, P. J., Bush, A. I., Martins, R. N., Masters, C. L., Rowe, C. C., Nathan, P. J., and Maruff, P. (2013) BDNF Val66Met, Abeta amyloid, and cognitive decline in preclinical Alzheimer's disease. *Neurobiol. Aging 34*, 2457−2464.

(35) Adamczuk, K., De Weer, A. S., Nelissen, N., Chen, K., Sleegers, K., Bettens, K., Van Broeckhoven, C., Vandenbulcke, M., Thiyyagura, P., Dupont, P., Van Laere, K., Reiman, E. M., and Vandenberghe, R. (2013) Polymorphism of brain derived neurotrophic factor influences beta amyloid load in cognitively intact apolipoprotein E epsilon4 carriers. *Neuroimage Clin 2*, 512−520.

(36) Devi, L., and Ohno, M. (2015) TrkB reduction exacerbates Alzheimer's disease-like signaling aberrations and memory deficits without affecting β-amyloidosis in 5XFAD mice. *Transl. Psychiatry 5*, e562.

(37) Chen, Q., Zhou, Z., Zhang, L., Wang, Y., Zhang, Y. W., Zhong, M., Xu, S. C., Chen, C. H., Li, L., and Yu, Z. P. (2012) Tau protein is involved in morphological plasticity in hippocampal neurons in response to BDNF. *Neurochem. Int. 60*, 233−242.

(38) Atasoy, I. L., Dursun, E., Gezen-Ak, D., Metin-Armagan, D., Ozturk, M., and Yilmazer, S. (2017) Both secreted and the cellular levels of BDNF attenuated due to tau hyperphosphorylation in primary cultures of cortical neurons. *J. Chem. Neuroanat. 80*, 19−26.

(39) Rohe, M., Synowitz, M., Glass, R., Paul, S. M., Nykjaer, A., and Willnow, T. E. (2009) Brain-derived neurotrophic factor reduces amyloidogenic processing through control of SORLA gene expression. *J. Neurosci. 29*, 15472−15478.

(40) Matrone, C., Ciotti, M. T., Mercanti, D., Marolda, R., and Calissano, P. (2008) NGF and BDNF signaling control amyloidogenic route and Abeta production in hippocampal neurons. *Proc. Natl. Acad. Sci. U. S. A. 105*, 13139−13144.

(41) Michalski, B., Corrada, M. M., Kawas, C. H., and Fahnestock, M. (2015) Brain-derived neurotrophic factor and TrkB expression in the "oldest-old," the 90+ Study: correlation with cognitive status and levels of soluble amyloid-beta. *Neurobiol. Aging 36*, 3130−3139.

(42) Castello, N. A., Green, K. N., and LaFerla, F. M. (2012) Genetic knockdown of brain-derived neurotrophic factor in 3xTg-AD mice does not alter Abeta or tau pathology. *PLoS One 7*, e39566.

(43) Chen, C., Wang, Z., Zhang, Z., Liu, X., Kang, S. S., Zhang, Y., and Ye, K. (2018) The prodrug of 7,8-dihydroxyflavone development and therapeutic efficacy for treating Alzheimer's disease. *Proc. Natl. Acad. Sci. U. S. A. 115*, 578−583.